JOURNAL OF PROPULSION AND POWER
Vol. 18, No. 2, March–April 2002

Massively Parallel Simulation of the Unsteady Flow in an Axial Turbine Stage

Jixian Yao*
Stanford University, Stanford, California 94305
Roger L. Davis†
United Technologies Research Center, East Hartford, Connecticut 06108
and
Juan J. Alonso‡ and Antony Jameson§
Stanford University, Stanford, California 94305

The results from two numerical simulations of the unsteady flow in a $1\frac{1}{2}$ stage axial-flow turbine are presented and compared with experimental data to show both the effect of blade count on the solution accuracy and the time-averaged and unsteady flow physics present. TFLO, the three-dimensional, multiblock, massively parallel turbomachinery flow solution procedure is used to simulate the flow through the Aachen 36-vane/41-blade/36-vane $1\frac{1}{2}$-stage turbine rig. Comparisons of the time-averaged and unsteady flow solutions of 1-vane/1-blade/1-vane and 6-vane/7-blade/6-vane configurations with the available experimental data are used to show the importance of matching actual blade counts in unsteady flow simulations as closely as possible. In addition, these comparisons are used to quantify the predicted aerodynamic performance differences and highlight the different unsteady flow physics in the two simulations.

Introduction

ACCURATE prediction of the flow physics in turbomachinery has been the subject of intensive research for many years. Unsteady flow phenomena in turbomachinery have especially been of great interest recently in an effort to improve aerodynamic efficiency, stability, and operability. Many large-scale computational fluid dynamics calculations have been made using descendants of Rai's code,[1] the MSU TURBO code,[2] Hah's code,[3] the CANARI code at the French National Aerospace Research Establishment (ONERA),[4,5] by researchers at the German Aerospace Center (DLR)[6] and the University of Stuttgart.[7] It is now possible with today's high-performance parallel computer systems to simulate the flowfield in turbomachinery with fewer assumptions and simplifications. Together with experimental investigations, numerical simulations can lead to a deeper understanding of the unsteady and time-averaged flows in turbomachinery and to subsequent improvements in turbomachinery design.

In an effort to stimulate the application of massively parallel computer systems and the development of numerical simulation tools that can take advantage of these systems, the U.S. Department of Energy (DoE) launched the Accelerated Strategic Computing Initiative. The three-dimensional, multiblock, parallel flow solver TFLO[8] has been developed under this initiative in an effort to step up to large-scale parallel steady and unsteady flow multistage turbomachinery simulations. The unsteady Reynolds-averaged Navier–Stokes equations are solved in the TFLO procedure using a cell-centered discretization on arbitrary multiblock meshes. The solution algorithm is based on an effcient implicit, dual time-step procedure[9] in which an explicit Runge–Kutta integration scheme coupled with multigrid, implicit residual smoothing and local time-stepping convergence acceleration techniques is used in an inner iteration for each time step. Wilcox's[10] k-ω two-equation turbulence model is used to predict the turbulence viscosity in the field. No turbulence transition model is introduced. The flow is assumed turbulent through the whole domain. The solver is parallelized using domain decomposition, a single program multiple data strategy, and the message passing interface standard. Unsteady multi-blade-row simulations are performed with the TFLO code using reduced integer blade counts that match or closely approximate those of the actual configuration.

In the current investigation the TFLO solution procedure has been used to investigate the unsteady flow through the Aachen $1\frac{1}{2}$-stage axial-flow turbine documented as an European Research Community on Flow, Turbulence, and Combustion (ERCOFTAC) benchmark test case. The experimental measurements were performed by Walraevens and Gallus.[11] Previous steady flow calculations have been reported by Emunds et al.,[12] and unsteady flow calculations have been reported by Walraevens et al.[13] and by Volmar et al.[14] Those investigations were mainly focused on the secondary flow features and used a single passage per blade row with either phase-lagged boundary conditions[15] or time inclining[16] to account for different airfoil counts in each blade row.

Unfortunately, even with large massively parallel computer systems, it is not always possible to simulate all of the blade passages included in the entire 360 deg of the turbomachine wheel. When the blade counts across the machine can be divided by some common factor, simulations can be executed with a reduced circumferential period that is common to all of the blade rows in the configuration. This reduced circumferential period is usually kept as small as possible in order to minimize the required computational resources. Frequently, however, it is not possible to come to some common circumferential period across the blade rows because of blade counts that are not divisible by a common factor. In this case the blade counts are modified as little as possible to allow a reduction in the solution domain. Because the airfoil loading of a given blade row is a function of the number of blades, different scaling strategies can

Received 21 May 2001; revision received 4 November 2001; accepted for publication 12 November 2001.

*Research Associate, Department of Aeronautics and Astronautics; currently Research Engineer, General Electric Company, 1 Research Circle, ES-209, Niskayama, NY 12309. Member AIAA.
†Senior Consulting Engineer, 411 Silver Lane. Member AIAA.
‡Assistant Professor, Department of Aeronautics and Astronautics. Member AIAA.
§T. V. Jones Professor of Engineering, Department of Aeronautics and Astronautics. Fellow AIAA.

be used on the airfoil to reduce the aerodynamic effect of changing the number of blades.

Unsteady multi-blade-row simulations are performed with the TFLO code using a reduced integer blade count for each blade row that closely provides for a common global circumferential pitch in all blade rows. To achieve an exact common global pitch, however, one or more of the blade rows must be scaled by the ratio of the actual blade count to the simulation blade count. In the current investigation airfoils to be modified as a result of a change in the blade count are scaled in the axial and circumferential directions in order to hold blade pitch/chord ratio and loading levels as consistent as possible with the original blade row. The advantage of the reduced integer blade count strategy is that storage requirements are kept to a minimum, inverse transformations are not required to postprocess the results, and low frequencies (below the first blade-passing frequency) are admitted, which can especially be important at off-design conditions.

To quantify the effect of using this type of blade count scaling on the accuracy of flow prediction, two different unsteady flow simulations have been performed. The simpler of the two simulations uses only one blade passage per blade row (1-1-1), and the more exact first-time simulation solves the flow in six passages in the first stator, seven passages in the rotor, and six passages in the second stator (6-7-6). Comparisons between the time-averaged solutions and experimental data show only minor differences in the pressure loading levels of each blade. In addition, the unsteady pressure envelopes of each blade row compare favorably between the two simulations. However, Fourier decompositions of the unsteady pressure fields show significant differences in the unsteady pressure amplitudes between the 1-1-1 and the 6-7-6 solutions. Similar findings have been found by Clark et al.[17] in an investigation of a $1\frac{1}{2}$-stage transonic turbine. As mentioned by Clark et al.,[17] the differences in harmonic amplitudes predicted by the simulations can be a significant factor in the accurate prediction of resonance stress levels on the blades. In addition, the current investigation has determined that the predicted relative total pressure losses can be significantly different because of the scaling strategy. Investigation of the unsteady relative total pressure loss field shows differences in the loss migration and mixing between the two simulations. These findings lead to the conclusion that the scaling factor used in these types of multi-blade-row unsteady flow should be kept to a minimum in order to predict accurately time-averaged total pressure losses and peak unsteady pressure loadings.

Aachen 1.5-Stage Axial Turbine

The Aachen turbine configuration is a subsonic axial-flow rig consisting of three blade rows: the first vane, the blade, and the second vane. The geometry of the second vane is exactly the same as that of the first vane. The exact blade counts for this case are 36, 41, and 36, respectively. The through flowpath is a parallel channel formed by the hub and casing with hub diameter of 490 mm and hub/tip ratio of 0.817. The geometrical parameters of the blades are described in Table 1. The geometry and experimental data package was provided by ERCOFTAC. There are two operating points given in the ERCOFTAC package, one with a lower mass flow rate (7 kg/s) and another with a higher mass flow rate (8 kg/s). The lower mass flow case is calculated in this paper. Steady total pressure, total temperature, flow angle, and velocity were taken at inlet, between blade rows, and at the outlet, but in different season when the rig was restarted. For this reason it is hard to obtain good comparisons at all axial stations with the results of a single simulation. The measured inlet total parameters, turbulence quantities, and exit backpressure are used as boundary conditions for the simulations. The flow in this turbine is significantly affected by various vortices in the blade passage as a result of its untwisted rotor and stator.

Table 1 Geometric parameters of the Aachen turbine

Parameters	Stator	Rotor
Chord, mm	62.0	60.0
Pitch chord ratio	0.77	0.67
Aspect ratio	0.887	0.917
Tip clearance, mm	——	0.4
Rotational speed, rpm	——	3500.0
Relative inlet flow angle,[a] deg	90.0	49.3
Relative outlet flow angle,[a] deg	20.0	151.2

[a]With respect to the circumferential direction.

A steady flow calculation was performed using a simple mixing plane between adjacent blade rows. This calculation served as a baseline for comparison with the unsteady flow solutions and the experimental data as well as the initial conditions for the unsteady flow simulations. The calculated mass flow rate is 7.127 kg/s.

Two unsteady flow calculations have been performed with different passage counts per blade row as already mentioned: the 1-1-1 and the 6-7-6 vane/blade/vane simulations. The unsteady flow solutions were time averaged over each global period to compare with the steady flow solution and experimental data. The unsteady flow solutions were also Fourier decomposed in an effort to understand the various unsteady pressure modes in the flow fields. The calculated mass flow rates are 7.148 and 7.147 kg/s for configurations 1-1-1 and 6-7-6, respectively.

Only the rotor blade is scaled for the following configurations. A comparison of the blade geometry is shown in Fig. 1, where the airfoils are aligned at the leading edges. Typical multiblock H-type mesh is used for all of the calculations. A separate block of mesh is generated for the tip gap region and is attached to the mesh of the main flowpath, as shown in Fig. 2.

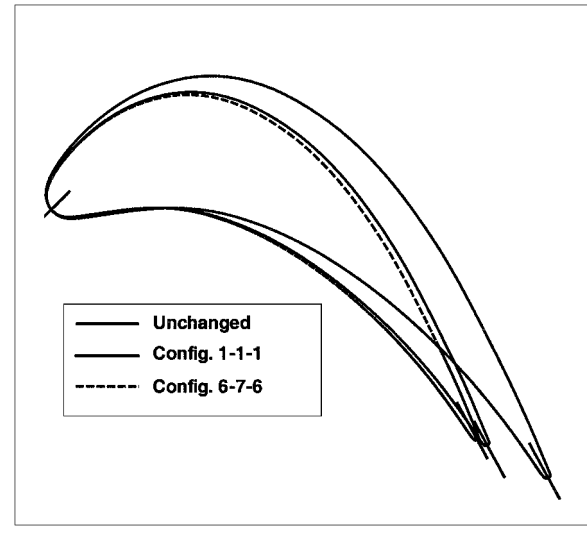

Fig. 1 Rotor geometry for different calculations.

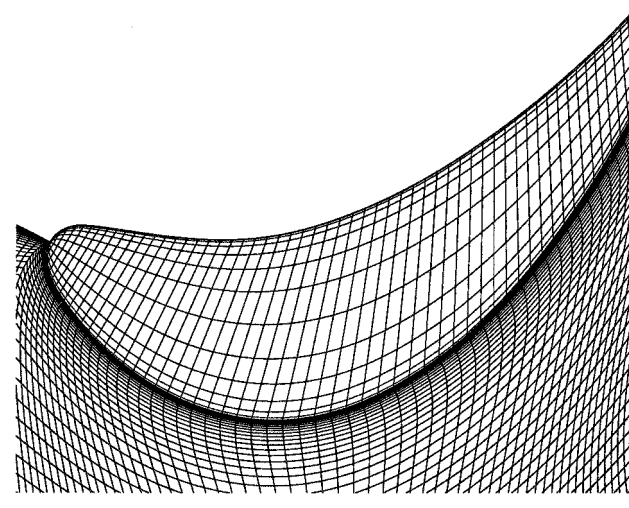

Fig. 2 Grid in the tip clearance of the rotor.

Configuration 1-1-1

This configuration consists of one blade passage per blade row, the geometry of the two vanes is kept unchanged, while the geometry of the blade is scaled to form 36 blade passages. Comparing to the original blade count of 41, the rotor blade is actually enlarged by 14%. The solidity is kept unchanged.

The mesh sizes used in this calculation can be summarized as follows: first vane, $137 \times 65 \times 81$; rotor, $113 \times 65 \times 81$ for the main passage and $89 \times 17 \times 17$ for the tip gap; stator, $153 \times 65 \times 81$. This resulted in a total of 2,147,516 points.

Configuration 6-7-6

Compared with the preceding configuration, this configuration consists of six passages for the first vane, seven passages for the blade, and six passages for the second vane. The geometry of the vanes are kept unchanged like in the 1-1-1 configuration, while the rotor blade is slightly shrunk by 2% to form a blade count of 42. This is the closest common blade count for this turbine rig. The grid sizes for each blade passage are the same as those of the 1-1-1 configuration. There are 19 blade passages, which leads to a total of 13,505,762 points.

Estimate of Computational Complexity

To resolve accurately the waveforms corresponding to the stator-rotor-stator interaction, a total of 100 time steps were used to rotate one blade past one vane passage. This resulted in the use of 700 time steps for one global period corresponding to $\frac{1}{6}$ of the turbomachine circumference. For each time step 30 multigrid cycles are performed to ensure the convergence of the inner iteration. The 6-7-6 simulation was executed on 187 processors of the DoE Blue Pacific IBM SP2 at Lawrence Livermore Laboratory. Each time step (with 30 inner iterations) required approximately 27.3 min including the computational and restart file input/output time. The 1-1-1 simulation was executed on 12 processors of an SGI Origin 2000. Each time step required approximately 46.6 min. The parallel computational effciency of the TFLO code for up to 1024 processors is documented in Ref. 18. Eleven global cycles (or 11 vane passings by the blade) were executed in order to reach a time periodic solution for the 1-1-1 configuration. Four global cycles (or 24 vane passings by the blade or 28 blade passings by a vane) were executed for the 6-7-6 configuration.

Time-Averaged Performance Parameters

The details of the time-averaged overall performance characteristics are discussed in this section. These time-averaged results, together with the results of a steady flow calculation, are compared to the experimental data available at 8.8 mm downstream of the trailing edges of the three blade rows.

Vane-1 Exit

A comparison between the predicted and experimental circumferentially averaged absolute total pressure at the exit of vane 1 (8.8 mm downstream of the trailing edge) is shown in Fig. 3. The inlet experimental total pressure profile, which was used in all of the simulations as an upstream boundary condition, is also included as a reference. Because there are no upstream blade rows to distort the flow, the total pressure profile at the exit of the first vane is flat across most of the span as expected. However, the secondary flows near both end walls distort the total pressure profile at 10% span near the hub and at 85% span near the tip.

The differences between the various predicted results are visible. The steady flow prediction matches the experimental data quite well in general with slight differences between 60 and 85% span. The location of both end-wall passage vortices is also predicted well. The time-averaged unsteady flow simulation for the 1-1-1 configuration predicts the tip passage vortex core location too far radially inwards. However, the total pressure profile from the same 1-1-1 simulation immediately downstream of the trailing edge agrees better with the experimental data. This indicates that the tip passage vortex shifts down 10% of the vane span and has a considerable amount of additional loss between 80 and 60% span. These effects are likely to be caused by the increase in the blade size for the 1-1-1 configuration. The configuration 6-7-6 clearly improves the prediction of this vortex core and the total pressure profile as well.

There is a strong total pressure loss around 10% span caused by the hub passage vortex. This vortex is captured by all of the simulations although in different intensity. The total pressure peak near 3% span is formed as a result of the fact that the hub passage vortex collects the low total pressure fluid in the inflow near the hub and pushes higher energy fluid downwards toward the end wall and hence forms the edge of the end-wall boundary layer. Unsteady calculations predict this peak very well, while the steady calculation tends to give a thicker end-wall boundary layer, which results in the predicted peak moving radially upwards.

Blade Exit

The comparison of absolute total pressure and total temperature at 8.8 mm downstream of the blade trailing edge is shown in Fig. 4. All of the predictions capture the spanwise trends of the experimental data. However, the absolute level of total pressure and total temperature is predicted lower than the measurement, which indicates more losses were generated by the calculations. The unsteady simulation of the 1-1-1 configuration predicts the total temperature peak location (measured at 72% span) below the experimental data as a result of the blade geometry change. The unsteady flow calculation of the 6-7-6 configuration, however, shows better agreement with the experimental temperature profile shape.

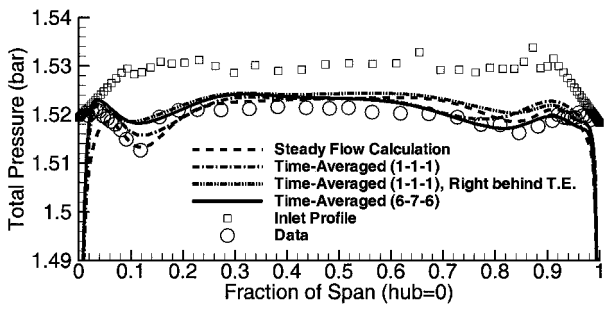

Fig. 3 Absolute total pressure comparison, 8.8 mm behind the trailing edge of vane 1.

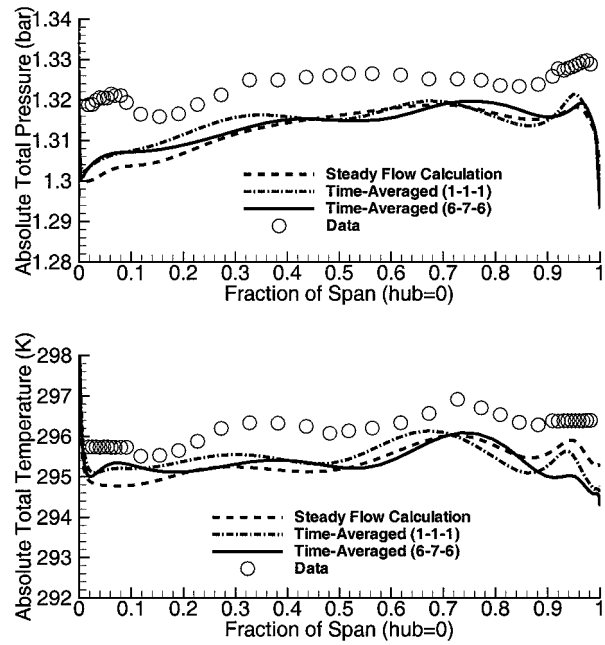

Fig. 4 Absolute total pressure and total temperature comparison, 8.8 mm behind the trailing edge of the rotor.

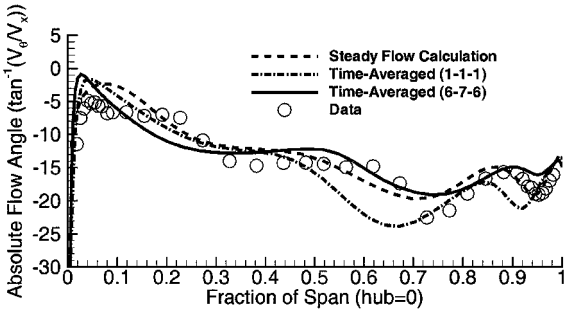

Fig. 5 Absolute flow angle comparison, 8.8 mm behind the trailing edge of the rotor.

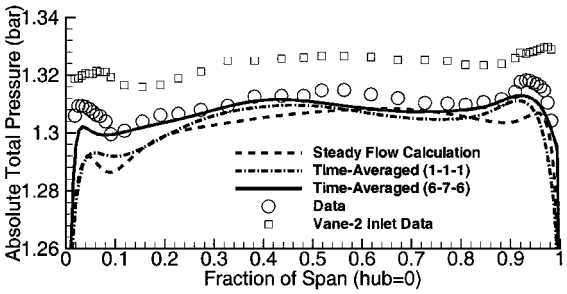

Fig. 6 Absolute total pressure comparison, 8.8 mm behind the trailing edge of vane 2.

The profile of the pitchwise absolute flow angle in Fig. 5 shows the different secondary flow signatures downstream of the trailing edge more clearly. The change in flow angle between 22–32% span is caused by the upstream vane hub passage vortex. Unfortunately, all of the simulations merge this upstream vane hub passage vortex with that of the rotor hub. The change in flow angle between 60–75% span is caused by the rotor trailing-edge vortex identified by Walraevens and Gallus.[11] This change in flow angle is captured well by the unsteady calculation for the 6-7-6 configuration, but the simulation underpredicts the strength. The simulation for the 1-1-1 configuration also captures this change in flow angle, but the spanwise location is too far inward radially. The change in flow angle between 90–95% span is caused by the upstream vane tip passage vortex and the rotor tip vortex. Again, the 6-7-6 simulation captures this flow angle change in the correct location, whereas the 1-1-1 simulation predicts the passage vortices at a lower span location.

Vane-2 Exit

The geometry of the second vane is identical to the first vane, but the second vane receives a much more distorted inflow resulting from the effect of the first vane and the rotor. Figure 6 shows comparable profiles to the ones behind the first vane. For comparison purposes the total pressure profile at the inlet to the second vane is included in this figure. The total pressure loss near the end walls results from the accumulation of loss from all of the blade rows. As before, the 6-7-6 configuration simulation significantly improves the prediction near the end walls (especially near the hub) over the 1-1-1 configuration and steady flow calculations as a result of the minimal geometry modifications and the modeling of the unsteady flow physics. Figure 7 shows two snapshots of the time-dependent secondary flow vectors at 0 and 75% rotor pitch, respectively, at the outlet of the passage. The rotor casing vortex (1) and the stator casing vortex (5) cause the total pressure dip at 80% span. The two hub passage vortices originated from the upstream rotor (2), and this stator (4) made a bigger dip on the total pressure profile at about 10% span. When the blade trailing edges line up at 0% rotor pitch (there is a 3-deg difference), the two predictions do not differ very much, however, at 75% rotor pitch; as a result of the much bigger change of pitch distance in configuration 1-1-1 (solidity is kept the same), the migration and merging of the vortices is considerably different.

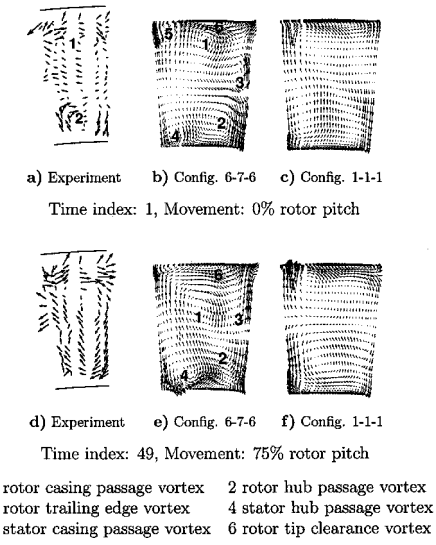

Fig. 7 Secondary flow at the outlet of vane 2.

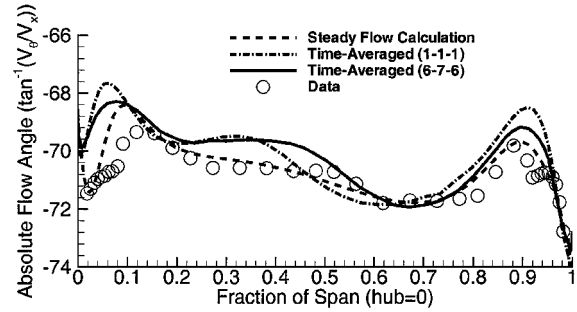

Fig. 8 Absolute flow angle comparison, 8.8 mm behind the trailing edge of vane 2.

Examining the inlet and exit total pressure measurements for the second vane, Fig. 6 shows that the peak loss at the inlet near the hub has been pushed towards the hub at the exit. The predictions recapture the dip of the total pressure. Most noticeably is the result of configuration 6-7-6 at 0 to 30% span from the hub, where it has a distinctive improvement of the total pressure. Near the casing area the radial movement of the loss core is just the opposite. The loss core has moved away from the end wall. The simulations predict this same characteristic.

The pitchwise absolute flow angle profiles at 8.8 mm behind the second vane trailing edge, however, are not that similar to the ones at the exit of the first vane as shown in Fig. 8. The changes in flow angle near the end walls are caused by the vane-2 hub and casing passage vortices and the upstream rotor passage vortices. The change in flow angle between 50–60% span is the signature of the rotor trailing edge vortex (3), which is carried through the second vane. All of the simulations do a reasonably good job at predicting the flow angle distribution with the time-averaged 6-7-6 solution being slightly better than the other two.

Unsteady Pressure on Blade Surfaces

The surface pressure distributions are of great importance for blade design. The time-averaged pressure distribution is important in terms of determining the "steady" forces and moments on each blade. The unsteady pressure forces, on the other hand, are critical in determining the maximum (peak) stress levels and whether any of the unsteady modes can lead to resonance.

The unsteady pressure envelopes at midspan are shown in Fig. 9. The rear part of the suction surface of the first vane has the largest pressure envelope for that blade row. The calculation of the 6-7-6 configuration shows a small but detectable difference compared with the result of the 1-1-1 configuration. The blade is affected throughout

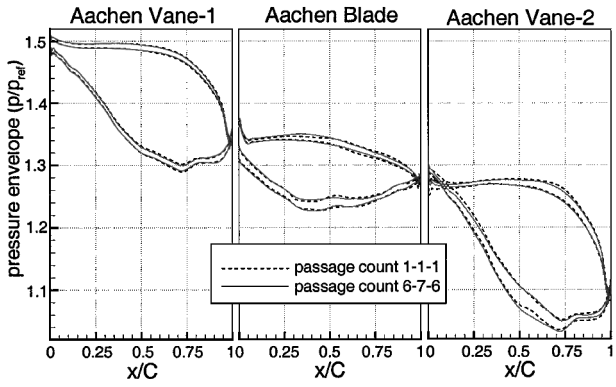

Fig. 9 Comparison of unsteady pressure envelopes at midspan.

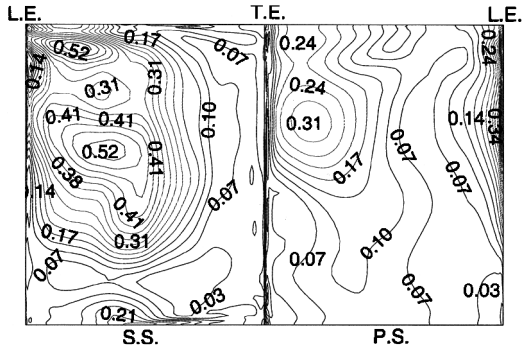

a) Config. 1-1-1

Config. 1-1-1 at 1BPF

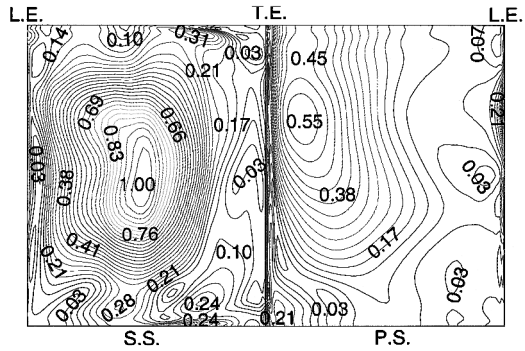

b) Config. 6-7-6

Config. 6-7-6 at 1BPF

Fig. 10 Comparison of normalized pressure amplitudes on vane-2 surfaces at 1BPF.

the whole surface as a result of the scaling difference of the two simulations. However, the pressure envelopes agree fairly well with each other. Interestingly, the 6-7-6 calculation shows a flatter profile on the blade suction surface than that of the 1-1-1 calculation. The envelope of the second vane shows a similar pattern to that of the first vane, but with a larger amplitude of pressure oscillations. Overall, the pressure envelopes of the two simulations are in fairly close agreement with each other. This would lead to the wrong conclusion that the blade count scaling differences between the two simulations did not result in much of a change in the unsteady pressure. As will be shown next, however, the frequency content and the unsteady pressure amplitudes can be quite different in the two simulations.

The second vane has exactly the same geometry as the first vane, but has quite different pattern of amplitudes when the rotor is scaled differently. This can be seen in Fig. 10, which shows the normalized amplitudes of the pressure oscillation on the suction and pressure surfaces of the second vane at one blade-passing frequency. The amplitudes are normalized by the maximum value of the whole spectrum of each blade row. Each blade is unfolded along the trailing-edge line for plotting purposes.

Unsteady Pressure Characteristics

The unsteady pressure signals in the flowfield are postprocessed using fast Fourier transforms (FFT) to obtain information in the frequency domain. We found that nonintegral blade-passing frequency (BPF) contents gain substantial power at various locations in the flowfield; we also discovered that subharmonics can become dominant in the spectrum when flow unsteadiness increase. These harmonics cannot be predicted using 1-1-1 configuration. These findings can benefit the reduced-order modeling method in terms of what frequency modes ought to be modeled (that is, those locally dominant nonintegral BPF contents and subharmonics need to be taken into account), but the challenge to that method is that the frequencies of those harmonics are not known a priori.

Inside the rotor passage the pressure field is greatly affected by the upstream and downstream stators as a result of interactions with the potential fields of both blade rows and the reflections that result. Figure 11 shows the FFT results of a point near the trailing edge at midspan on the pressure surface of the blade for both the 6-7-6 and 1-1-1 simulations. It indicates not only that the 6-7-6 spectrum has much more frequency content but also that the amplitudes of the fundamental frequencies are quite different from those predicted in the 1-1-1 simulation. The 1BPF harmonic of the 1-1-1 simulation is

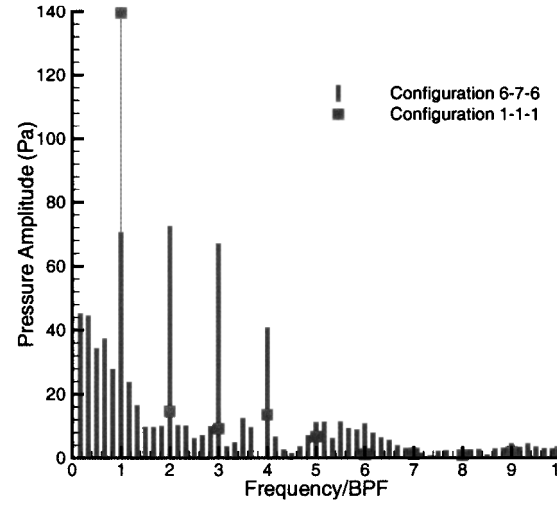

Fig. 11 Pressure harmonics of a point at midspan, near trailing edge of rotor pressure surface.

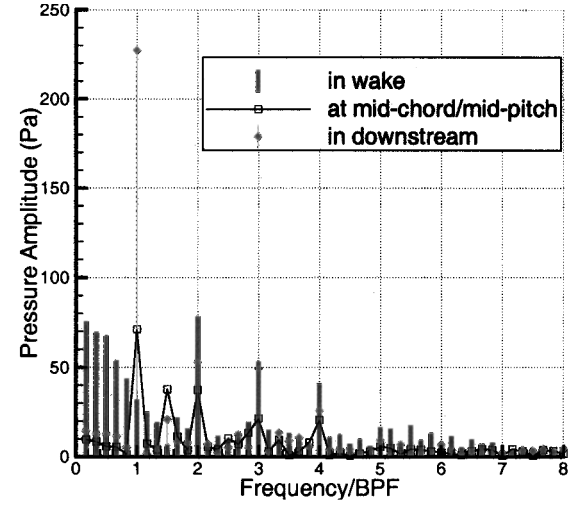

Fig. 12 Pressure harmonics of the rotor at midspan, configuration 6-7-6.

twice that of the 6-7-6, but the second, third, and fourth harmonics are quite small relative to those of the 6-7-6 simulation. Clearly, this shows that the local unsteady pressure amplitudes can vary significantly because of blade scaling.

On the other hand, the subharmonics predicted by the 6-7-6 simulation are observed to have different magnitudes at different places. Figure 12 shows the FFT results of the pressure spectra of three representitive points at midspan. In the wake region, while the amplitude at 1BPF loses dominance, the subharmonics gain significant power and reaches the same level of harmonic at 2BPF. In the downstream of the rotor, the 1BPF harmonic regains power as a result of the passing blades of the downstream stator. Also the harmonic is at 1.5BPF in the middle of the passage. This harmonic gains more power when approaching casing where the flow is affected by the tip gap leakage flow. Figure 13 shows the pressure spectra at different locations at midpitch near casing. At 75% chord and downstream the harmonics at 1BPF and 1.5BPF dominate the spectra. At 100% chord the 1.5BPF harmonic becomes the only dominating power as the 1BPF and 2BPF harmonics drop into noise level. Again, this is a feature that cannot be predicted by 1-1-1 configuration.

The subharmonics get even stronger in the third blade row (vane 2). Figure 14 shows the FFT of the pressure spectra in upstream, in the passage, and in the wake at 80% span. This figure shows that the subharmonics can be stronger than the 2BPF, and in extreme they are the dominating harmonics in the wake. The harmonics at 1.3BPF grow even greater in magnitude than that in the first vane. This

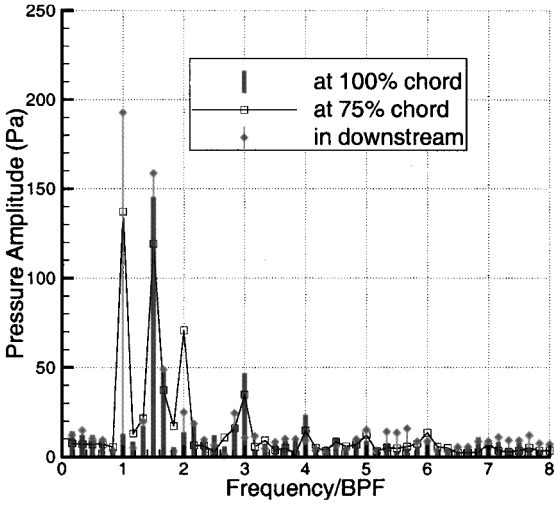

Fig. 13 Pressure harmonics of the rotor at midpitch nearing casing, configuration 6-7-6.

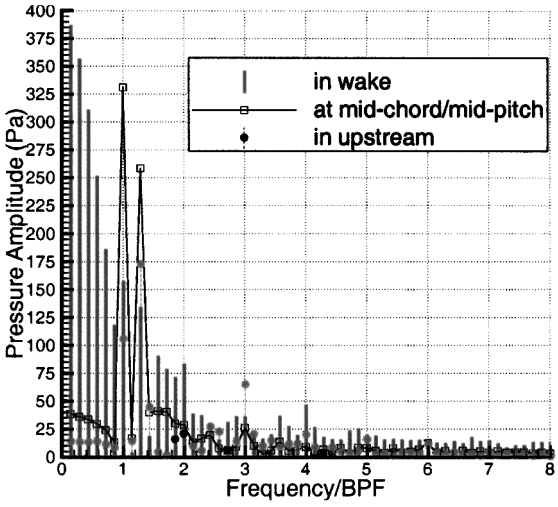

Fig. 14 Pressure harmonics of vane 2 at 80% span.

capturing of nonintegral blade-passing frequencies is not related to the trailing-edge vortex shedding whose frequency is at least a magnitude higher than the blade-passing frequency. It represents the longer period (more than one passage) pressure waves reflecting and being broken down between the blade rows.

The propagation of pressure waves in the axial gap is also investigated using spatial FFT, which suggests that pressure waves decay slower when blade count is closer to the real geometry.

Conclusions

An investigation in which two unsteady numerical simulations of a $1\frac{1}{2}$-stage axial subsonic flow turbine using 1-1-1 and 6-7-6 blade counts are compared with each other as well as with time-averaged and unsteady experimental data has been presented. This investigation suggests the following:

1) Blade scaling can affect the accuracy of predictions in a considerable amount for both time-averaged performances and unsteady flows, especially in the frequency contents. Excessive change in blade geometry contaminates the prediction accuracy of unsteady flow simulations.

2) The dominating modes in the unsteady flowfields shift significantly at different locations. Subharmonics and nonintegral blade-passing frequencies gain substantial power in the wakes, in the tip clearance, in the axial gaps, where most of the flow unsteadiness occur. These frequencies can only be predicted accurately if the blade counts of each blade row are modeled precisely. Hence, it is important to minimize the airfoil scaling necessary to achieve a common circumferential period in order to accurately predict the unsteady pressure wave amplitudes that are required for accurate prediction of peak (resonance) stress levels of the blades.

3) Configuration of one passage per row leads to loss of subharmonics and nonintegral blade-passing frequency contents, which could dominate or have significant power in the whole spectrum, especially in wakes and in tip gaps.

4) The time-averaged pressure and unsteady pressure envelopes are not significantly affected by the blade count scaling strategy providing that the blade scaling is not excessive (that is, $<14\%$ for this case).

5) The preceding findings could provide essential information to the reduced-order simulation method in terms of the frequency contents that need to be modeled for increased accuracy.

The use of large-scale, massively parallel computer systems is making it possible to simulate true blade counts over increasing numbers of blade rows in a turbomachine. New Reynolds-averaged Navier–Stokes solution procedures, such as TFLO, are continuing to be developed to take advantage of these computer systems, validated, and demonstrated for large-scale turbomachinery applications.

Acknowledgments

The authors would like to thank the U.S. Department of Energy for its generous support under the Accelerated Strategic Computing Initiative program. The authors would especially like to recognize the support of the staff and the Lawrence Livermore National Laboratory. We would also like to thank the managers at United Technologies Research Center and Pratt and Whitney for their support. The European Research Community on Flow, Turbulence and Combustion is also gratefully acknowledged for providing the experimental data package for the Aachen case.

References

[1] Rai, M. M., "Three-Dimensional Navier–Stokes Simulations of Turbine Rotor-Stator Interaction," NASA TM 100081, March 1988.

[2] Chen, J. P., and Briley, W. R., "A Parallel Flow Solver for Unsteady Multiple Blade Row Turbomachinery Simulations," *Journal of Turbomachinery*, American Society of Mechanical Engineers, Paper 2001-GT-348, Vol. 115, No. 2, 1993, pp. 240–248.

[3] Copenhaver, W. W., Hah, C., and Puterbaugh, S. L., "Three-Dimensional Flow Phenomena in a Transonic High-Through-Flow Compressor Stage," *Journal of Turbomachinery*, Vol. 115, No. 2, 1992.

[4] Rouzaud, O., and Plot, S., "Numerical Simulations of Unsteady Internal Flows Using Dual Time Stepping Method," 1st International Conference on CFD, Tech. Rept., July 2000.

[5]Billonnet, G., Fourmaux, A., and Toussaint, C., "Evaluation of Two Competitive Approaches for Simulating the Time-Periodic Flow in an Axail Turbine Stage," *4th European Conference on Turbomachinery Fluid Dynamics*, Tech. Rept., ATI-CST-008/01, March 2001.

[6]Engel, K., Eulitz, F., Pokorny, S., and Faden, M., "3D Navier–Stokes Solver for the Simulation of the Unsteady Turbomachinery Flow on a Massively Parallel Hardware Architecture," *Notes on Numerical Fluid Mechanics, Vol. 52, Flow Simulation with High-Performance Computers II*, edited by E. H. Hirshel, Springer-Verlag, Berlin, 1996, pp. 117–133.

[7]Jung, A. R., Mayer, J. F., and Stetter, H., "Unsteady Flow Simulation in an Axial Flow Turbine Using a Parallel Implicit Navier–Stokes Method," *High Performance Computing in Science and Engineering '98*, edited by E. J. Krause and W. Jager, Springer-Verlag, Berlin, 1999, pp. 269–294.

[8]Yao, J., Jameson, A., Alonso, J. J., and Liu, F., "Development and Validation of a Massively Parallel Flow Solver for Turbomachinery Flows," AIAA Paper 00-0882, Jan. 2000.

[9]Jameson, A., "Time Dependent Calculations Using Multigrid, with Applications to Unsteady Flows past Airfoils and Wings," AIAA Paper 91-1596, June 1991.

[10]Wilcox, D. C., *Turbulence Modeling for CFD*, DCW Industries, Inc., La Cañada, CA, 1998.

[11]Walraevens, R. E., and Gallus, H. E., "Three-Dimensional Structure of Unsteady Flow Downstream the Rotor in a 1-1/2 Stage Turbine," *Unsteady Aerodynamics and Aeroelasticity of Turbomachines*, edited by Y. Tanida, and M. Namba, Elsevier Science B. V., Amsterdam, Tokyo, 1995, pp. 481–498.

[12]Emunds, R., Jennions, I. K., Bohn, D., and Gier, J., "The Computation of Adjacent Blade-Row Effects in a 1.5 Stage Axial Flow Turbine," American Society of Mechanical Engineers, Paper 97-GT-81, June 1997.

[13]Walraevens, R. E., Gallus, H. E., Jung, A. R., Mayer, J. F., and Stetter, H., "Experimental and Computational Study of the Unsteady Flow in a 1.5 Stage Axial Turbine with Emphasis on the Secondary Flow in the Second Stator," American Society of Mechanical Engineers, Paper 98- GT-254, June 1998.

[14]Volmar, T. W., Brouillet, B., Gallus, H. E., and Benetschik, H., "Time Accurate 3D Navier–Stokes Analysis of a 1-1/2 Stage Axial Flow Turbine," AIAA Paper 98- 3247, July 1998.

[15]Erdos, J. L., Alzner, E., and McNally, W., "Numerical Solutions of Periodic Transonic Flow Through a Fan Stage," *AIAA Journal*, Vol. 15, No. 1, 1977, pp. 1559–1568.

[16]Giles, M. B., "UNSFLO: A Numerical Method for Unsteady Inviscid Flow in Turbomachinery," Massachusetts Inst. of Technology, Gas Turbine Lab. 195, Cambridge, MA, Oct. 1988.

[17]Clark, J. P., Stetson, G. M., Magge, S. S., Ni, R. H., Jr., Haldeman, C. W., Jr., and Dunn, M. G., "The Effect of Airfoil Scaling on the Predicted Unsteady Loading on the Blade of a 1 and 1/2 Stage Transonic Turbine and a Comparison with Experimental Results," American Society of Mechanical Engineers, Paper 2000-GT-0446, May 2000.

[18]Yao, J., Jameson, A., Alonso, J. J., and Liu, F., "Development and Validation of a Massively Parallel Flow Solver for Turbomachinery Flows," *Journal of Propulsion and Power*, Vol. 17, No. 3, 2001, pp. 659–668.